Influence of relative humidity upon pollution and dust during ACE-Asia: Size distributions and implications for optical properties

S. G. Howell, A. D. Clarke, Y. Shinozuka, V. Kapustin, C. S. McNaughton, and B. J. Huebert

School of Ocean and Earth Science and Technology, University of Hawaii at Manoa, Honolulu, Hawaii, USA

S. J. Doherty and T. L. Anderson

Department of Atmospheric Sciences, University of Washington, Seattle, Washington, USA

Received 30 December 2004; revised 5 July 2005; accepted 21 September 2005; published 24 March 2006.

[1] An extensive set of aerosol physical and optical measurements was taken over the waters east of Asia during the Aerosol Characterization Experiment-Asia (ACE-Asia) project in the spring of 2001. Dust storms upwind of the study area combined with intense pollution plumes from coastal cities yielded an opportunity to examine both types of aerosol, in isolation and as they interacted. Scattering calculated from aerosol size distributions measured with an optical particle counter agreed well with simultaneous nephelometer measurements. We periodically heated sample air to evaporate sulfates and organic material. The change in volume upon heating agreed well with simultaneous measurements of aerosol composition. This volatile material was distributed on dust in rough proportion to surface area. Here we use the particle size and composition data to improve estimates of scattering at ambient humidity and to examine the effects of mixing on the optical properties of both pollution and dust aerosols. The presence of dust results in uptake of soluble and condensible species onto its surface and thereby reduces the mass scattering efficiency of the pollution aerosol by 50% and suppresses the change in scattering due to relative humidity (f(RH)) by up to 35%.

Citation: Howell, S. G., A. D. Clarke, Y. Shinozuka, V. Kapustin, C. S. McNaughton, B. J. Huebert, S. J. Doherty, and T. L. Anderson (2006), Influence of relative humidity upon pollution and dust during ACE-Asia: Size distributions and implications for optical properties, *J. Geophys. Res.*, *111*, D06205, doi:10.1029/2004JD005759.

1. Introduction

[2] Scattering of sunlight by atmospheric aerosols exerts a significant, though poorly quantified cooling effect on climate [*Intergovernmental Panel on Climate Change*, 2001]. Aerosols are particularly challenging for models and remote sensing since they have relatively short lifetimes, are heterogeneously distributed vertically and horizontally, and their physical and optical properties are strongly influenced by their composition and environment. Including realistic aerosol behavior in climate models adds considerably to their complexity and computational demands [e.g., *Adams and Seinfeld*, 2002]. One difficulty is that the optical properties of aerosols are strongly influenced by relative humidity (RH). Hygroscopic materials in the particles attract water, causing particles to grow and mean refractive index to drop, even at humidities well below saturation. The degree of growth and resulting optical changes are functions of particle composition, size and shape.

[3] This hygroscopic growth has a significant effect on the radiation balance because of several competing effects [*Im et al.*, 2001; *Markowicz et al.*, 2003]. As particles grow, scattering increases, but backscatter fraction decreases and single scattering albedo increases. In addition, humidity growth is a complicating factor when trying to characterize aerosol size distributions from satellites [*Kapustin et al.*, 2006].

[4] Many experiments have quantified particle growth with relative humidity (often called g(RH)) or the resultant changes in scattering (referred to as f(RH)). g(RH) is typically measured with humidified tandem differential mobility analyzers (hTDMAs), which use one DMA to select a single particle size at low humidity and a second to measure the size changes after humidification [e.g., *Rader and McMurry*, 1986; *Pitchford and McMurry*, 1994; *Massling et al.*, 2003]. This technique is limited to particles with dry diameter $D_p \leq 0.25$ μm so the humidified particles remain small enough to be measured with the second DMA. f(RH) is typically measured using paired nephelometers, one dry and the other fitted with a scanning humidifier [e.g., *Carrico et al.*, 2003], though it has been done with a single scanning RH nephelometer [*Kotchenruther et al.*, 1999].

[5] Two aerosol size modes typically dominate scattering. Dust and sea salt make up the coarse mode, with mass

0148-0227/06/2004JD005759$09.00

median diameter >1 μm. Dust is insoluble so absorbs little water and has *f*(RH) between 1.0 and 1.1 [*Twomey*, 1977; *Li-Jones et al.*, 1998]. In contrast, sea salt is by definition soluble and exhibits a large *f*(RH). Another mode, with dry mass median diameter typically between 0.2 and 0.4 μm, often called the accumulation mode, is composed of soots from both biomass and fossil fuel combustion, fly ash, soluble inorganic salts, and a variety of organic compounds. Water uptake by the inorganic salts are well characterized from electrodynamic balance studies. Fly ash and soot are insoluble, so take up very little water. The organic component comprises a highly variable fraction of the aerosol and its hygroscopic behavior varies from nearly hydrophobic to almost indistinguishable from soluble salts [*Ming and Russell*, 2002]. As a general rule, fresh urban aerosol tends have very low *g*(RH) [*Gasparini et al.*, 2004] while natural aerosols and aged anthropogenic particles in the accumulation mode tend to be quite hygroscopic [*Pitchford and McMurry*, 1994].

1.1. Aerosol Characterization Experiment-Asia (ACE-Asia)

[6] The Aerosol Characterization Experiment-Asia (ACE-Asia) field campaign [*Huebert et al.*, 2003] took place in late March through May of 2001 and involved 3 aircraft, 2 ships, and a number of ground sites. It was designed to look at the variety of aerosols advecting from Asia over the Pacific Ocean and timed to coincide with the plumes of dust that are produced every spring from the Gobi and Taklamakan deserts in Central Asia. In addition, the prevailing westerlies bring pollution from coastal cities out over the ocean. The primary goals of the experiment were to characterize sources, composition, and optical effects of the aerosol. Considerable efforts were made to coordinate our in situ sampling with satellite measurements and chemical transport models, both as validation exercises and to aid in modeling the impact of the aerosols on climate.

[7] The measurements we use here were performed aboard the NSF/NCAR EC-130Q aircraft. During 19 research flights we found a wide variety of aerosols including relatively clean free tropospheric and marine boundary layer air, dust plumes at a variety of altitudes and impressive plumes of pollution. Aircraft-based measurements have some great advantages over surface-based sampling, including the ability to sample over a relatively large area and to make vertical profiles. Unfortunately, the mobility of aircraft is largely incompatible with time-consuming measurements like those for *f*(RH) and *g*(RH). The limited duration of flights means only a few measurements can be made, and the high speed means that either sample air must be held in the plane for long periods [*Kotchenruther et al.*, 1999], or risk that the air at the end of the sampling period is utterly different than that at the beginning, rendering the data useless. This is a difficulty for integrated samples such as filters for chemical analysis, but is exacerbated with *g*(RH) and scanned *f*(RH), since the individual measurements are not averages but a series of instantaneous measurements assumed to represent the entire period.

[8] Much of the data used here has been presented elsewhere and is available at http://www.joss.ucar.edu/codiac/. Here we focus on the optical consequences of the interaction between dust and pollution. In the ACE-Asia study region, pollution is often emitted into very dusty air. This is in contrast to Saharan dust detected over the tropical North Atlantic, where pollution sources are generally upwind of the dust-producing areas. In the absence of dust, pollutants such as sulfates, nitrates, and organic matter are typically found in the accumulation mode (roughly 0.08–0.5 μm). When dust is present, some fraction of this material is diverted to the coarse mode dust [*Tang et al.*, 2004; *Kline et al.*, 2004; *Clarke et al.*, 2004]. Because mass scattering efficiency in the accumulation mode is higher than that for coarse particles, we expect that the dust reduces the scattering due to pollutants, and hence their radiative forcing. Our objective is to quantify this effect under the circumstances commonly observed in ACE-Asia, with pollution emitted into a dusty atmosphere.

1.2. Definitions of Diameter

[9] Particle size distributions shown here were measured with an optical particle counter (OPC), which was chosen because it spans the range of optically important particle sizes (0.1 to 12 m) at a fairly high sampling rate (30 s). However, it is important to recognize that particle size typically depends on the measurement technique used. When examined through an electron microscope [e.g., *Gao and Anderson*, 2001; *E. A. Reid et al.*, 2003], it is clear that most dry particles cannot be effectively described by a single diameter. In addition, no single representation of diameter can account for a particle's mass, surface area, and optical properties. In this work we deal with three commonly used versions of diameter: optical diameter (D_o), the diameter of a sphere of known refractive index that scatters light as efficiently as the particle in question; aerodynamic diameter (D_{ae}), the diameter of a particle of unit density that settles as quickly as the particle being measured; and volume-based diameter (D_v), which is the diameter of a spherical particle with the same volume. For homogeneous, spherical particles of known density and refractive index, one can transform between definitions:

$$D_v = D_{ae}\sqrt{\frac{C(D_{ae})}{\rho_p C(D_v)}} \tag{1}$$

and

$$D_v^2 Q_{\mathrm{scat}}(D_v, m_{\mathrm{chem}}, \lambda_{\mathrm{OPC}}) = D_o^2 Q_{\mathrm{scat}}(D_o, m_{\mathrm{OPC}}, \lambda_{\mathrm{OPC}}) \tag{2}$$

where ρ_p is particle density, $C(D)$ is the Cunningham slip correction factor, m is the complex refractive index $n + ik$, λ is wavelength, and Q is the Mie scattering efficiency. (Note that an implied $\rho_{ae} = 1$ in the numerator makes the radical unitless.) For nonspherical particles, correction factors χ are customarily introduced to give

$$D_v = D_{ae}\sqrt{\frac{\chi_{ae} C(D_{ae})}{\rho_p C(D_v)}} \tag{3}$$

and

$$D_v^2 Q_{\mathrm{scat}}(D_v, m_{\mathrm{chem}}, \lambda_{\mathrm{OPC}}) = \chi_o D_o^2 Q_{\mathrm{scat}}(D_o, m_{\mathrm{OPC}}, \lambda_{\mathrm{OPC}}) \tag{4}$$

[10] While equations (1) and (3) are single valued functions, neither side of equations (2) and (4) are, so transformations are necessarily approximate. To make things even more complicated, D_v and D_{ae} are unambiguous properties of a particle (though not easily measured), but D_o depends on the wavelength λ used and on the angular scattering range measured.

[11] Largely because of these difficulties, *J. S. Reid et al.* [2003] recommend eschewing D_o as poorly defined and unreliable for practical use, which they defined as determining mass-size distributions and mass scattering efficiencies. However, for climate modeling in general and for ACE-Asia in particular, the aerosol optical properties themselves are of prime interest. One consequence of sizing particles on the basis of scattering is that the effects of asphericity, inhomogeneity and varied refractive indices in the aerosol particles are included in the sizing. That makes calculation of D_v difficult, but means that the diameters returned by the OPC (D_o), are well suited for calculating scattering because all of those irregularities are included in the measurement. Therefore, despite the limitation of D_o, we will show that it is a useful quantity for assessing optical properties.

2. Methods

[12] Scattering and absorption measurements aboard the C-130 were described by *Anderson et al.* [2003]. Briefly, two TSI, Inc. model 3563 nephelometers measured scattering, while two Radiance Research particle soot absorption photometers (PSAPs) measured absorption. An impactor was used to limit one of the nephelometers and one of the PSAPs to fine particles only (D_{ae} < 1 μm). Two Radiance Research model M903 nephelometers were used to measure f(RH). One (henceforth labeled RRwet) was downstream of a humidifier, which usually maintained the RH at the inlet of the nephelometer at 85%. Another RH sensor mounted immediately downstream of RRwet averaged 2% higher RH, with a standard deviation of 2%, suggesting that RH change within the nephelometer were small. RH in the other (called RRdry) was uncontrolled, though the cabin temperature of the plane was warmer than ambient, so RH was typically below 10% (55% of the time) and rarely exceeded 40% (<5% of the time overall and <8% when below 2 km.

[13] Sample air for the nephelometers and PSAPs entered the aircraft through a low-turbulence inlet (LTI), that enhanced large particle collection efficiency [*Huebert et al.*, 2004b]. This enhancement, combined with losses in sample tubing inside the aircraft, had only a small net effect (<10%) on overall scattering [*Anderson et al.*, 2003].

[14] Aerosol size distributions were measured with a LAS-X optical particle counter (OPC), custom modified with a wide-span log amplifier and a 256 channel pulse height analyzer [*Clarke*, 1989]. Sample air was not RH controlled, but was diluted with an equal amount of desiccated and filtered air to keep humidity low (generally between 20 and 30%) to minimize the effect of water uptake. During level legs, sample air was periodically diverted through tubes heated to 150°C and 300°C. Changes in particle volume due to this heating has been shown to correspond to sulfuric acid and ammonium sulfate in the clean marine boundary layer [*Clarke*, 1991], but in the more complex environment of ACE-Asia, interpretation of this volatility is less straightforward.

[15] Ionic composition of the aerosol was measured with two complementary techniques: a Particle Into Liquid Sampler (PILS) accepted particles up to about 1.3 μm and cycled every 4 min [*Lee et al.*, 2003]. Size resolved inorganic ion data come from a Micro-Orifice Impactor (MOI, made by MSP), but samples were taken only on extended level legs and mechanical problems limited the quality of the data [*Kline et al.*, 2004]. Although ion ratios as a function of size are accurate, the size distributions are poorly defined and useful mainly to differentiate coarse from fine composition. Both the PILS and MOI sampled through LTIs.

[16] The Elemental and Organic Carbon (EC and OC) measurements are described in detail by *Huebert et al.* [2004a] and *Ding et al.* [2002]. Sample air was brought in through a solid diffuser inlet, passed through a virtual impactor to enhance particle concentration and reduce organic vapor, put through an carbon-impregnated denuder to eliminate organic vapor, then particles were collected on baked quartz fiber filters, and OC that evaporated from the filter was captured on a carbon-impregnated glass fiber filters (CIGs). Analyses for EC and OC were performed with a thermal desorption method using optical absorption to differentiate between OC and EC. In addition, FTIR measurements for organic functional groups were performed [*Maria et al.*, 2003]. While not providing direct OC quantification, this technique can be used to estimate the ratio of organic carbon to total organic material (OM), and can suggest whether the OM is hydrophilic or not (on the basis of C = 0 versus C-H bond occurrences). Neither the EC/OC nor the FTIR systems used air from the LTI, but from a solid diffuser inlet that appears to perform well with wet aerosols as large as 2 μm and dust aerosols to at least 6 μm [*Huebert et al.*, 2004b]. As we expect that most OC, and nearly all EC are found on smaller particles, inlet losses are not likely to be significant. The relatively low supermicrometer absorption measured with the PSAPs confirms that only ~20% of the BC is associated with dust even at very high dust loadings [*Clarke et al.*, 2004].

3. Results

[17] The scattering and absorption measurements have been reported by *Anderson et al.* [2003] and *Doherty et al.* [2005] while chemical composition has been described by *Lee et al.* [2003], *Kline et al.* [2004], *Huebert et al.* [2004a], and *Maria et al.* [2003] so those results are not presented individually here. Size distributions were discussed by *McNaughton et al.* [2004], but that work concentrated on nucleation, so the emphasis was on smaller particles. A more extensive discussion of size distributions can be found in work by *Clarke et al.* [2004], which concentrates on the optical role of dust and soot-containing particles.

[18] One minute averages of f(RH) and altitude for the entire field phase are shown in Figure 1. As expected for dust, f(RH) was minimal when coarse particles dominated scattering. (Sea salt was seldom a large fraction of the coarse aerosol.) f(RH) for dust-dominated aerosol appears to be 1.1 to 1.5 at all altitudes. A striking feature of Figure 1 is the absence of high f(RH) at high altitude even when fine

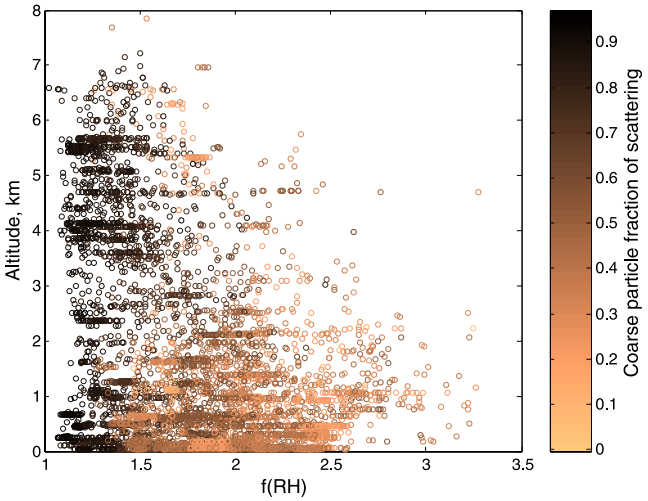

Figure 1. Variation of *f*(RH) with altitude and dust. Coarse mode scattering fraction is used here as a proxy for dust concentration. Data shown are all 60 s averages with b_{sp} > 10 Mm^{-1}.

particles dominate scattering, a feature also noted by *Doherty et al.* [2005]. The transition appears to occur between 2 and 4 km. While the data are sparse, there is evidence that the ratio of carbon to sulfate is higher in the free troposphere [*Huebert et al.*, 2004a], so *f*(RH) of OM may dominate in the FT. This is consistent with *Kotchenruther et al.* [1999], who found similar behavior over the U.S. east coast.

3.1. OPC Size Distributions and Nephelometry

[19] One of the benefits of the extensive instrumentation aboard the C-130 is a certain degree of redundancy, where the same aerosol characteristics are examined with more than one technique. This enables us to check for consistency between data sets. One such closure test is to examine whether the size distributions as measured by the OPC successfully account for the measured optical properties.

[20] Figure 2 shows one of the comparisons between OPC and nephelometer. Since the diameters returned by the OPC are really optical diameters, we use the refractive index of the latex spheres rather than of the actual particles to calculate scattering. To make the most direct comparison possible, we used the raw data from the nephelometer and used the OPC distributions to calculate the scattering the nephelometer should sense, given its geometry [*Anderson and Ogren*, 1998]. Mie calculations were performed with code adapted from *Bohren and Huffman* [1983].

[21] Table 1 shows a more extensive comparison, including the other wavelengths, backscattering, and the submicrometer nephelometer. The effect of the impactor was modeled with a functional fit from *Winklmayr et al.* [1990]:

$$E = 1 - \left[1 + (D_{50}/D_{ae})^{2s}\right]^{-1} \quad (5)$$

where D_{50} is the 50% cut diameter (0.996), D_{ae} is the aerodynamic diameter of the particle, and s is the slope (5.0). We use equation (3), assuming that particles have a shape correction factor χ_{ae} = 1.4 [*J. S. Reid et al.*, 2003] and a density of ~2.7 g/ml (on the basis of typical densities for dust components: clay minerals typically 2.6–2.8, calcite 2.71, calcium sulfate 2.3 to 2.8 (depending on hydration state), and 2.25 to 3.1 for common aluminosilicates [*Weast et al.*, 1989]), which yields $D_g \approx D_{ae}/0.7$. This is a rough approximation, but imprecision does not greatly affect the results, since the region around 0.7 μm is typically a minimum in the volume and area distributions. By coincidence, sea salt particles behave similarly, as after drying they have ρ = 2.2 and $\chi_{ae} \approx 1.1$.

[22] While the total scattering slopes are excellent and correlation coefficients generally remain near 0.95, there are some discrepancies. The low calculated backscatter is most likely a result of aspherical particles with enhanced backscatter relative to spheres. The trend in the submicrometer slopes suggests that either the impactor is modeled incorrectly or that the OPC is undersizing small particles. These minor discrepancies aside, it is clear that the OPC size distributions can be used to accurately calculate total scattering, if not an accurate phase function for large particles. This good agreement across a wide range of aerosol types and particle sizes strongly suggests that particle transmission efficiency to the OPC, which was not directly measured, was not significantly different than

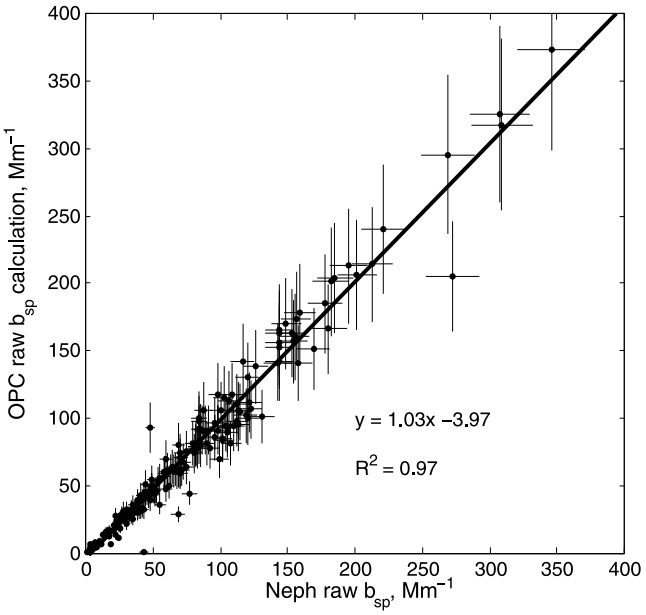

Figure 2. Comparison of scattering coefficients measured by the TSI total nephelometer and calculated from OPC size distributions at λ = 0.55 μm. The nephelometer data are uncorrected for truncation area, and scattering calculations are integrated over the angular sensitivity of the nephelometer [*Anderson and Ogren*, 1998]. Data are for all level legs of the project. Horizontal bars indicate uncertainty range of the nephelometer measurements [*Anderson and Ogren*, 1998], excluding the angular truncation error, yielding errors near 7%. Error estimates for the scattering calculations from size distributions are difficult to perform, but estimates from Monte Carlo calculations suggest that variations on the order of 15–20% are reasonable [*Clarke et al.*, 2002].

Table 1. Comparisons Between OPC and Nephelometer

	Total Scattering		Backscattering	
λ, nm	Slope	R^2	Slope	R^2
		All Aerosol		
450	1.00	0.95	0.82	0.95
550	1.00	0.95	0.82	0.96
700	1.03	0.95	0.86	0.95
		Submicrometer Aerosol		
450	0.98	0.97	1.07	0.97
550	0.94	0.95	1.03	0.96
700	0.90	0.91	1.02	0.94

that to the nephelometers, at least over the particle size ranges most important for scattering.

3.2. Size Distributions and Absorption

[23] Unlike scattering, OPC data cannot be used directly to calculate absorption. In addition, closure exercises are difficult because the complex refractory indices for soot [*Fuller et al.*, 1999] and dust [e.g., *Kalashnikova and Sokolik*, 2002] are not well known. Instead, we have shown in a separate paper [*Clarke et al.*, 2004] that the size distributions can be used to calculate effective indices of refraction when constrained by the absorption and scattering data.

3.3. Size Distributions and Volatility

[24] Figure 3 illustrates the effect of dust on size distributions and volatility. Figure 3a shows pollution with very minor amounts of dust present. The continuous line is the unheated size distribution and shows a pronounced accumulation mode centered at 0.3 μm and a low, broad coarse mode. The dashed line is the remainder after heating to 300°C. The coarse material that remains after heating is primarily dust, though sea salt is also present. The fine mode is a combination of soot, fly ash, and refractory organic material [*Clarke et al.*, 2004]. The volatile volume is the difference between the two curves and is composed of sulfates, nitrates, and volatile organic material (see section 3.3).

[25] Under dusty conditions (Figure 3b), volume is almost completely dominated by supermicrometer dust particles, so the accumulation mode and volatile fraction are difficult to see. With only the volatile material shown (Figure 3c), the effect of dust on the volatile material is obvious: much of the volatile material has migrated to the coarse mode and that remaining in the accumulation mode has a smaller diameter.

[26] The dust line in Figure 3c exaggerates the volatile volume due to three influences: thermophoretic losses as the air cools down from 300°C, losses of large particles due to the slightly more complex tubing through the heated inlet, and the tendency of D_o to overestimate D_v, particularly for large, nonspherical particles. While the last problem is difficult to constrain, it is possible to quantify the effects of the first two by looking at very dusty distributions (>200 μm^3 cm^{-3}) showing very little accumulation mode volatile material (<6 μm^3 cm^{-3}). Under those circumstances, the refractory distributions averaged 91 ± 4% of the unheated ones for all particle sizes >0.7 μm, despite the lack of significant volatile material. Therefore we divide the 300°C distributions by 0.91 for all sizes to correct for thermophoretic and other tubing losses. The effect of the correction is shown as the "corrected" line.

[27] While the displacement of volatile material from the accumulation mode to dust particles is strikingly evident in the size distributions, quantifying the volatile volume on the large particles is subject to large uncertainties and so must be regarded as only semiquantitative. In addition to the particle sizing and transmission efficiency uncertainty mentioned above, volatile deposits are likely to change the shape of particles. Nevertheless, the data appear to be useful for addressing the mechanism of deposition. If the only important limitation is diffusion, then the amount of volatile material a depositing on a spherical particle is

$$J_a = 2\pi D_p d_a c_a \tag{6}$$

where J_a is molar deposition rate, D_p is particle diameter, d_a is the diffusion constant, and c_a is the concentration of a (adapted from *Seinfeld and Pandis* [1998, equation 11.12]). Thus deposition rate is proportional to the diameter of the particle. If deposition of volatile material is limited by a reaction occurring in the particle, then since mass of reactant depends on the mass of the particle, deposition should be proportional to mass.

[28] In Figure 4, we assume that the refractory size distribution represents primary aerosol. The coarse mode is dust (or sea salt) and the fine mode is soot, fly ash, and possibly refractory organics that condense on soot in or near exhaust pipes and chimneys. The fraction of volatile material deposited on the dust fraction is nearly proportional to

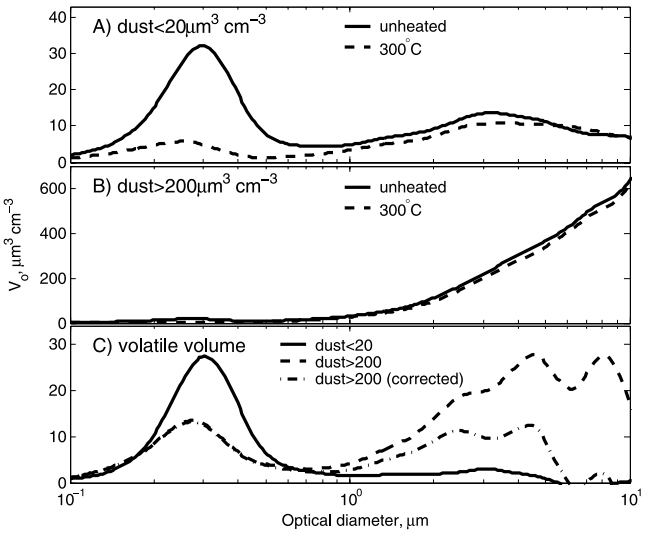

Figure 3. Size distributions and volatility with and without dust. Dust causes volatile material to be displaced onto the dust mode. V_o is particle volume based on optical diameter. It is likely to be an overestimate for aspherical particles, particularly large dust. The "corrected" volatile distribution in Figure 3c compensates for thermophoretic and tubing losses (see text). The low-dust line is the average of 2.9 hours of data from nine flight legs, while the high-dust line represents 4.4 hours from eight flight legs.

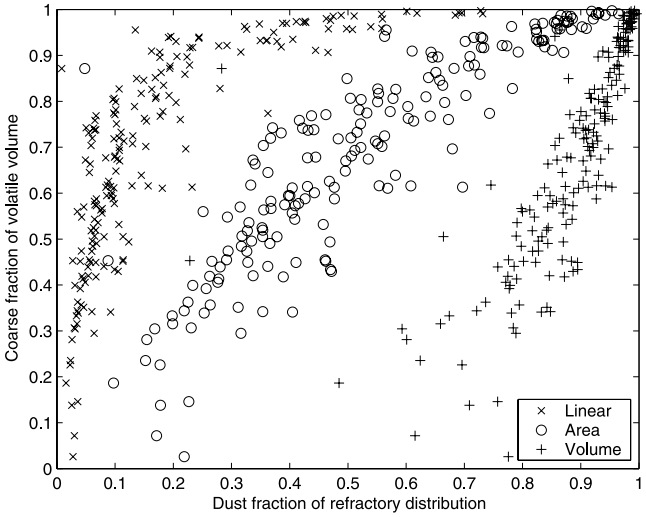

Figure 4. Distribution of volatile material between dust and submicrometer refractory material. The same data are plotted three ways; in each case, the *y* axis is the fraction of volatile material present on the dust mode up to 5 μm, while the *x* axis is the fraction of dust diameter, area, or volume in the refractory size distributions.

the area of the particles rather than diameter or volume, as would be the case with the mechanisms mentioned above. This suggests that neither mechanism dominates or that deposition is limited by surface binding or reaction sites.

3.4. OPC Volatility and Chemical Composition

[29] In the remote marine boundary layer, volatile material as determined by the OPC has been shown to correlate well with chemical composition. In particular, volume reduction between unheated and 150°C reflect sulfuric acid and between 150 and 300°C are equal to ammonium sulfate plus ammonium bisulfate [*Clarke*, 1991]. As the aerosol was much more complex during ACE-Asia, volatility cannot be so simply interpreted. However, comparisons of OPC volatility with inorganic ions and organic material show that volatility is closely related to composition even in this region.

[30] Figure 5 shows such a comparison for all of the level legs during the project. Several assumptions were necessary:.

[31] 1. Ammonium ions were first allocated to create NH_4HSO_4.

[32] 2. Any remaining ammonium was converted NH_4HSO_4 to $(NH_4)_2SO_4$.

[33] 3. Any remaining sulfate was assumed to be H_2SO_4. This ignores the reaction of sulfate with dust to form $CaSO_4$, which is probably not volatile at 300 o C. However, $CaSO_4$ is only slightly soluble, and it is not clear to what extent either PILS or the MOI detect it.

[34] 4. Any remaining ammonium was allocated to NH_4NO_3.

[35] 5. Any remaining nitrate was assumed to be associated with dust particles as $Ca(NO_3)_2$ and nonvolatile. This is because the size-resolved MOI data showed that NO_3^- was generally associated with dust except when sufficient NH_4^+ was present to fully neutralize $SO_4^=$ [*Kline et al.*, 2004].

[36] 6. The OPC size distributions had to be convoluted with the PILS sampling efficiency curve, which had a 50% size cut at $D_{ae} \approx 1.3$ μm [*Lee et al.*, 2003].

[37] 7. 50% of the organic matter was assumed to be volatile at 300°C. During the Indian Ocean Experiment (INDOEX) project, OC was determined by measuring CO_2 evolution while heating in the presence of oxygen [*Mayol-Bracero et al.*, 2002] and roughly half of the total was found by 300°C. OC measurements during ACE-Asia were made while heating under He, so were not comparable to conditions in the OPC. If one assumes that between 30 and 70% of OM evaporates at 300°C, the associated error in volatile volume would be 5 to 15%.

[38] 8. Particles are internally mixed homogeneous spheres with refractive indices equal to the volume-average refractive index of the chemical constituents. This is not in fact true for most particles, particularly when soot is present, but we have insufficient knowledge about particle morphology to perform more detailed calculations. Volume-averaging soot can dramatically change absorption [*Fuller et al.*, 1999], though that effect appears to be minor for particles <0.7 μm. Inhomogeneous refractive indices in nonabsorbing spheres appear to behave similarly to homogeneous spheres, but suppress some resonances, thus smoothing the Mie curves [*Chen et al.*, 2003]. The effect of asphericity is likely to cause large errors in volume and hence mass for large particles, as mentioned by [*J. S. Reid et al.*, 2003], but the PILS size cut limits that error.

[39] With these assumptions and approximations, it is clear from Figure 5 that the measured species largely account for the volatility found with the OPC. The slope is near 1 and the intercept is near zero. Thus we can conclude that the OPC volatility measurement is indeed an indicator of the species normally associated with pollu-

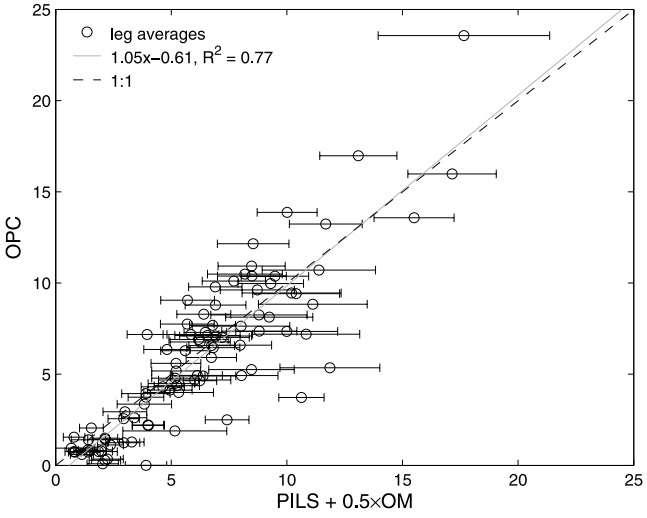

Figure 5. Comparison between volatile volumes determined chemically (PILS + OM/2) and with the OPC. Units are $mm^3\ m^{-3}$. Error bars are the square root of the sum of the squares of the estimated PILS error (30%) and half of the OM error (reported by sample). The latter is an underestimate, as uncertainties in density, volatility, and OM:OC are not included.

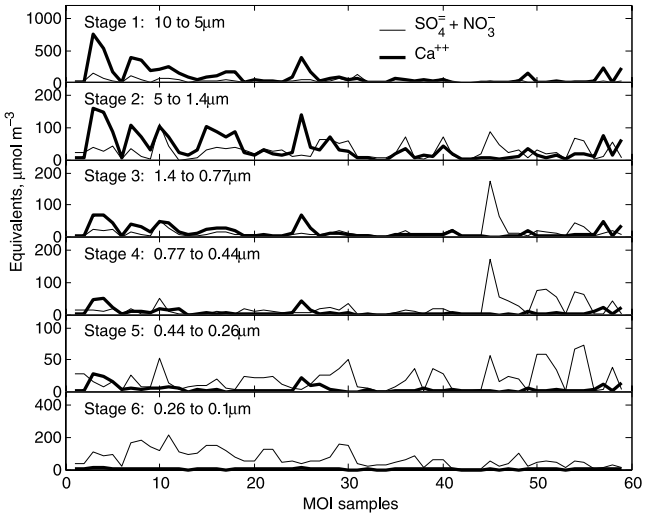

Figure 6. Calcium as a neutralizing agent for nitrate and sulfate in the impactor data. Note that the anions are often correlated with but rarely exceed soluble calcium in stages 1–3, which are typically dominated by dust.

tion. It also gives us some confidence that the volumes we determine optically are not beset by large artifacts because of inhomogeneity, asphericity, or inaccurate refractive index calculations. Of course, this agreement is valid only for the relatively small particles sampled by the PILS, leaving large-particle volatile volumes poorly constrained.

4. Discussion

[40] There are two obvious ways that redistributing sulfates, nitrates, and organic material from the accumulation mode to larger particles can affect *g*(RH) and thus *f*(RH). The first is simply mass transfer to larger particles, which have lower mass scattering efficiencies and lower *f*(RH) at constant *g*(RH). Another effect can be that reactions with dust may produce salts less hygroscopic than the acids and ammonium salts prevalent in submicrometer aerosol. In particular, sulfuric and nitric acids can react with calcium carbonate to form $CaSO_4$ and $Ca(NO_3)_2$, which are only slightly soluble. While $CaSO_4$ is uncommon in the dust source regions and in high-altitude dust plumes lacking much pollution, much of the $CaCO_3$ in the original dust has reacted to form $CaSO_4$ in the polluted marine boundary layer [*Winchester and Ming-Xing*, 1989]. There is also evidence of these reactions in the MOI data, where NO_3^- was usually associated with large particles [*Kline et al.*, 2004]. During strong dust episodes, a significant fraction of the $SO_4^=$ was found on large particles as well. Figure 6 hints that sulfate and nitrate concentrations on dust may be limited by soluble calcium, suggesting that virtually all of the sulfate and nitrate are reacted and thus insoluble. Thus dust may have very low affinity for water even when soluble material is deposited.

4.1. Direct Measurements of *f*(RH)

[41] One of our particular interests in this project was to determine how the presence of dust affects the optical properties of the pollution. While we periodically switched a 1 m impactor in line with the *f*(RH) nephelometers, that was not an effective way to isolate dust from pollution, as the tail of the dust distribution was frequently responsible for much of the submicrometer scattering [*Clarke et al.*, 2004] and any sulfates that wound up on dust were excluded. Another means to separate dust from pollution is required. We chose to estimate the pollution contribution using submicrometer absorption. Figure 7 demonstrates that at very low dust levels, scattering due to pollution in this region is strongly related to submicrometer absorption with a slope $m_{sa} = 7.4 \pm 0.4$. Since Asian dust absorbs light relatively poorly [*Anderson et al.*, 2003] submicrometer absorption is likely to be a good indicator of pollution regardless of dust concentration. Some soot certainly ends up on large dust particles, but that appears to be a small fraction of the total (up to 20% at dust loadings of 600 μg m^3) [*Clarke et al.*, 2004].

[42] We can take advantage of the relationship between scattering and absorption to determine the effect of dust on *f*(RH) due to pollution alone. Wet and dry scattering σ can be split into pollution and dust components:

$$\sigma_{tw} = \sigma_{pw} + \sigma_{dw} \tag{7}$$

$$\sigma_{td} = \sigma_{pd} + \sigma_{dd} \tag{8}$$

where the first subscript refers to total, pollution, or dust and the second to dry or wet. Defining *f*(RH) due to pollution as $f_p = \frac{\sigma_{pw}}{\sigma_{pd}}$, that due to dust as $f_d = \frac{\sigma_{dw}}{\sigma_{dd}}$ and taking advantage of the relationship $\sigma_{pd} = m_{sa} b_{ap}$ from Figure 7, one can derive

$$f_p = \frac{\sigma_{tw} - f_d(\sigma_{td} - m_{sa} b_{ap})}{m_{sa} b_{ap}} \tag{9}$$

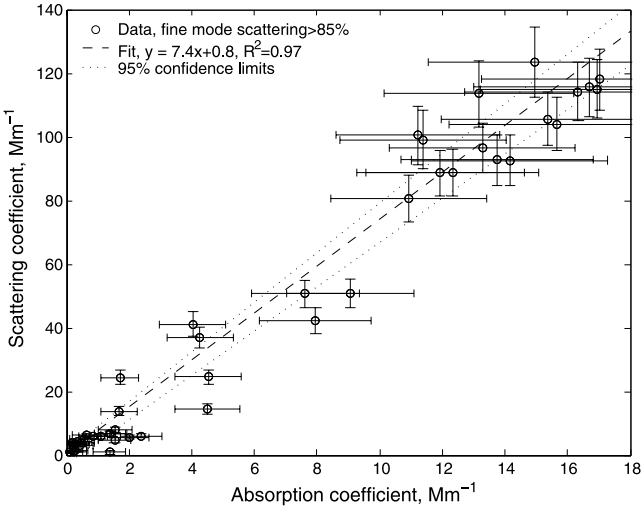

Figure 7. Relationship between scattering (RRdry) and submicrometer absorption coefficients at very low dust levels (defined as fine mode fraction of scattering >85%). The uncertainty in the slope is 0.4. PSAP errors, calculated from *Bond et al.* [1999], are dominated by a 20% method accuracy uncertainty.

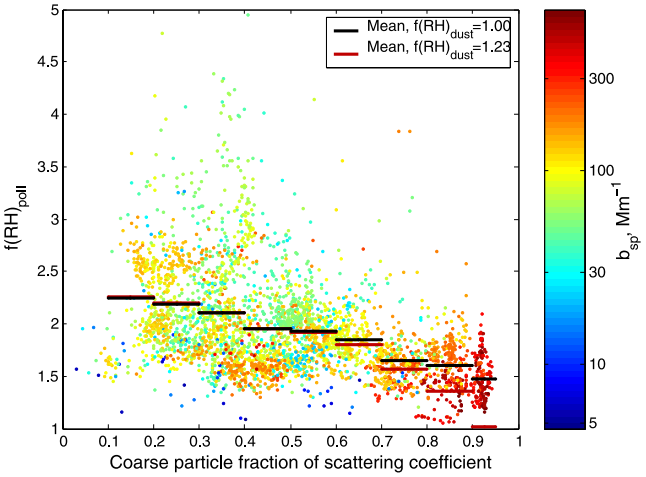

Figure 8. Apparent *f*(RH) of pollution as affected by dust (equation (10)). Black horizontal bars are mean values within the span, while the red bars are the mean values assuming $f_d = 1.23$ (equation (9)). The data are color coded by total scattering. All data below 2 km are included.

If we assume water does not deliquesce on dust, then $f_d = 1$ and equation (9) becomes

$$f_p = \frac{\sigma_{tw} - \sigma_{td}}{m_{sa} b_{ap}} - 1 \tag{10}$$

[43] Figure 8 shows the results of equation (10). While there is significant scatter, there is a clear downward trend in f_p as dust assumes a greater fraction of scattering, with the mean dropping from 2.3 to 1.5. If $f_d > 1$, then the apparent effect on f_p is even greater. As an extreme case, the gray bars show the result of equation (9) assuming $f_d = 1.23$, the mean *f*(RH) during the most dust-dominated periods. In that case, the hygroscopic growth due to dust is entirely suppressed. Since f_p at very high dust concentrations never exceeded the mean f_p at low dust concentrations, a more reasonable conclusion is that $f_d \approx 1$ and *f*(RH) is due exclusively to the volatile matter.

[44] It has been noted in other work [*Doherty et al.*, 2005] that the *f*(RH) values found on the C-130 are lower than those measured aboard the R/V *Ronald H. Brown* [*Carrico et al.*, 2003]. As the shipboard measurements were performed carefully by experienced personnel with more sophisticated humidification equipment, this naturally casts some doubt on the numbers presented here. 1°C heating in the nephelometer sensing volume would drop our humidity from 85 to 80% and thus drop apparent *f*(RH) by ~35%, which would be sufficient to erase the discrepancy, but seems unlikely, as sensors at the inlet and outlet actually recorded a slight RH increase (averaging 2% with a standard deviation of 2%). It is conceivable that a degree of heating occurred but was masked by cooling within the 3 cm of plumbing between nephelometer and sensor, but the nephelometer was insulated (by a pile of sweaters) to prevent that problem.

[45] Another possible source of this disagreement is our use of Radiance Research nephelometers, which are poorly characterized compared with the TSI versions used by [*Carrico et al.*, 2003]. As noted by *Anderson et al.* [2003], RRdry systematically reported smaller scattering values than the TSI nephelometers on board, ranging from 10 to 30% lower as the fraction of scattering due to coarse particles increased. Only about 1/3 of this difference could be explained by increased truncation error in the RR nephelometer. The remainder of the discrepancy is not adequately accounted for, but might be due to nonideal distribution of light from the flash lamp. Whatever the cause, *f*(RH) can still be measured accurately if the errors do not significantly increase as the particles grow. One recent laboratory study that employed both TSI and RR nephelometers showed little difference in measured *f*(RH) but the size distributions, centered at about 0.2 μm, were smaller than those measured in ACE-Asia [*Kus et al.*, 2004].

4.2. Calculations of *g*(RH)

[46] For particles big enough (>50 nm) that the Kelvin effect due to curvature is negligible, *g*(RH) is a function only of composition, not particle size. We assume that the sulfate and nitrate salts measured with the PILS and MOI are hygroscopic, as are the sodium and chloride from sea salt. The refractory material is assumed to be nonhygroscopic. That leaves the organic matter, which is difficult to model as aerosol organic matter has been reported with a wide range of hygroscopicity. Modeling of hygroscopic growth using the functional group analysis mentioned earlier suggests that *g*(RH) is enhanced roughly 2% when organic matter solubility is included as compared with the assumption that it is completely insoluble (S. Maria and L. M. Russell, personal communication, 2002). We've chosen a very crude approximation for current purposes: we assume all of the volatile material grows as effectively as the salts measured with the PILS. Since the volatile material contains roughly half of the total organic material, that is effectively assuming that half of the organic matter is hygroscopic while the other half is not.

[47] We use the so-called ZSR scheme to determine water uptake from the PILS inorganic ion measurements [*Cohen*

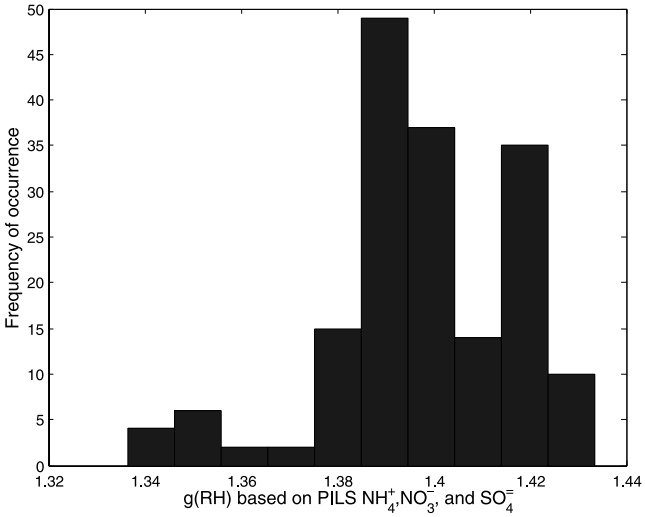

Figure 9. Histogram of *g*(RH) calculated from PILS data.

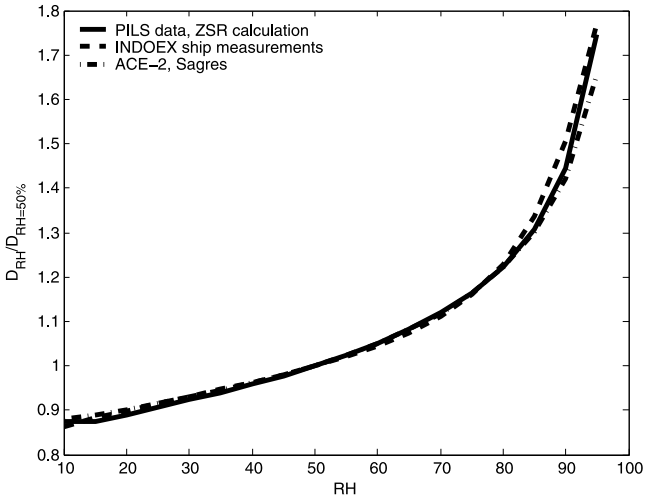

Figure 10. Plot of *g*(RH) from various earlier experiments. Since authors use different "dry" humidities, this plot has been normalized to *g*(RH) = 1 at 50% RH. Data from INDOEX are from the "most hygroscopic mode" [*Massling et al.*, 2003], while ACE-2 is from pollution episodes at Sagres [*Swietlicki et al.*, 2000].

et al., 1987; *Howell and Huebert*, 1998]. It uses water activity from binary solutions of varying concentration to determine water activity of multiple-electrolyte solutions. Figure 9 shows the range of variations in *g*(RH) calculated from the PILS data. It is a very narrow range, reflecting the dominance of ammonium sulfate under most conditions.

[48] This calculated growth agrees closely with some measurements in polluted marine boundary layers in earlier experiments (Figure 10). However, this shows only the most hygroscopic modes, ignoring the nonhygroscopic components. If the refractory material and the volatile organic matter are completely insoluble, *g*(RH) is reduced by as much as 40%.

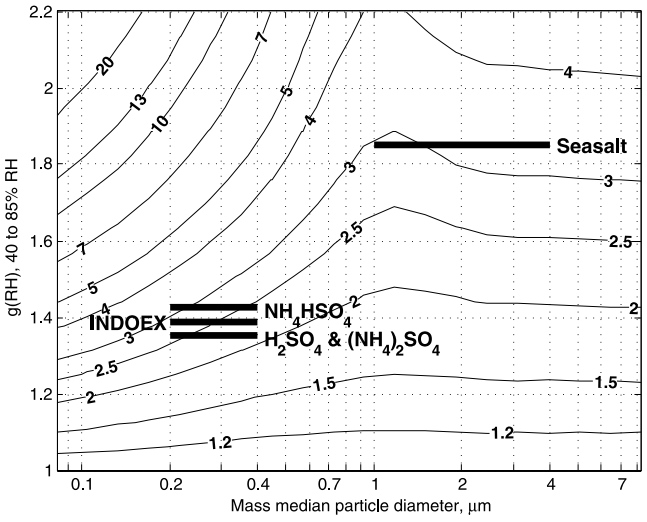

Figure 11. Contours of *f*(RH) as a function of particle diameter and *g*(RH). Distributions are lognormal, geometric standard deviation is 1.5, and dry refractive index is 1.50.

Table 2. Fitted Lognormal Parameters Used in *f*(RH) Model[a]

	N_p	D_m	σ_g
Soot	370	0.16	1.5
Dust	22	0.64	2.8
Volatile	730	0.22	1.3

[a] N_p is the number of particles in the mode, D_m is the median diameter, and σ_g is the geometric standard deviation. Dust parameters are fits of the median of the 34 dustiest legs (V_o > 100 m^3 cm^{-3}). Soot and volatile material fits were from the 27 high-pollution legs (>4 μg $SO_4^=$ m^{-3}) without high dust.

4.3. Size Distributions and *f*(RH)

[49] *f*(RH) is a function of particle size distribution, particle growth, and refractive index. Figure 11 shows an example of the relationship given some simplifying assumptions: particles are homogeneous spheres; dry refractive index is 1.50; wet refractive index is a volume-weighted mean between dry refractive index and water; and distributions are lognormal with geometric standard deviation of 1.5. As particle diameter grows large, *f*(RH) approaches $g(RH)^2$, simply reflecting growth in cross-sectional area. For very small particles, *f*(RH) can be very large, as scattering goes with the 4th power of diameter.

[50] A few interesting areas are superimposed on the contours. *g*(RH) for sulfuric acid and ammonium salts [*Cohen et al.*, 1987] and sea salt [*Tang et al.*, 1997] are shown in the regions where those mass distribution peaks are typically located. Sea salt shows twice the diameter growth, but its larger particle size yields a smaller *f*(RH) difference. Also shown is the mean *g*(RH) for the most hygroscopic mode of 0.25m INDOEX aerosol as measured on the R/V *Ronald Brown* [*Massling et al.*, 2003]. Since there was significant organic material on those particles [*Mayol-Bracero et al.*, 2002], it is interesting to note that the net water uptake was similar to that of pure sulfates. Many particles did grow less, indicating that less hygroscopic material was often present as well.

[51] It should be noted here that the choice of dry refractive index has a significant and counterintuitive effect: as the particle is diluted with water, the refractive index drops, partially counteracting the growth. This effect is stronger when starting from a higher refractive index, so *f*(RH) is smaller. In Figure 11, this means that sea salt *f*(RH) (n_{dry} = 1.57) is overestimated while sulfuric acid is underestimated and ammonium sulfate salts are about right.

[52] Because of the semiquantitative nature of the volatile volume on the coarse mode, direct calculations of *g*(RH) and *f*(RH) at high dust concentrations are impractical. Therefore we use a simple model to explore the effect of dust on scattering and *f*(RH) due to pollution. Table 2 shows lognormal modes used in the model as fitted to data from the OPC. The amount of pollution (soot + volatile material) is assumed to be constant. The median diameter and geometric standard deviation of the dust remain constant, but the number ranges from 0 to the maximum value of 22. A mass of volatile material proportional to the dust surface area is removed from the dustless volatile distribution and allocated to the area mode of the dust, as suggested by

Figure 4. As RH changes, all of the volatile material gains water as in Figure 9, increasing particle size and reducing refractive index.

[53] The effect of increasing dust on scattering is shown in Figure 12. While the total amount of volatile material remains constant, the scattering due to the volatile material drops by 50%, reflecting the reduced mass scattering efficiency at larger diameters. While dust strongly reduces the scattering efficiency of the volatile material, the effect on overall scattering is a relatively modest 10% drop. Figure 13 shows the modeled effect of dust on *f*(RH) together with measured values for all level legs during ACE-Asia. While the data follow the overall pattern of the model, neither curve fits the data very well. The 25 to 80% curve (which assumes 1 o heating in the nephelometer) is generally than the 25 to 85% curve. The effect of dust is less than 20% when dust is less than about 70% of the refractory volume.

5. Conclusions

[54] During ACE-Asia, we encountered a wide variety of air masses including mixtures of dust and pollution. The presence of dust altered the size distribution and perhaps the composition of the pollution, reducing both the scattering due to pollution by up to 50% and the enhancement of that scattering at high humidity by as much as 40%. While the scattering effectiveness of the pollution was reduced under dusty conditions, the effect on overall scattering was modest, at 10% or less because of the overwhelming scattering of the dust itself. Some enhancement of scattering at high humidity was always detectable, even in the dustiest conditions, but there was always enough hygroscopic volatile material present to account for that enhancement; there is no evidence that the dust itself was hygroscopic.

[55] Despite the theoretical difficulties with diameters as determined from optical particle counters, retrieved size distributions allow us to calculate scattering well for submicrometer particles. Errors are larger for dust-dominated size distributions. Volatility measurements reflected chemical composition effectively for small particles. In the presence of dust, volatile matter partitioned between dust and soot approximately according to surface area.

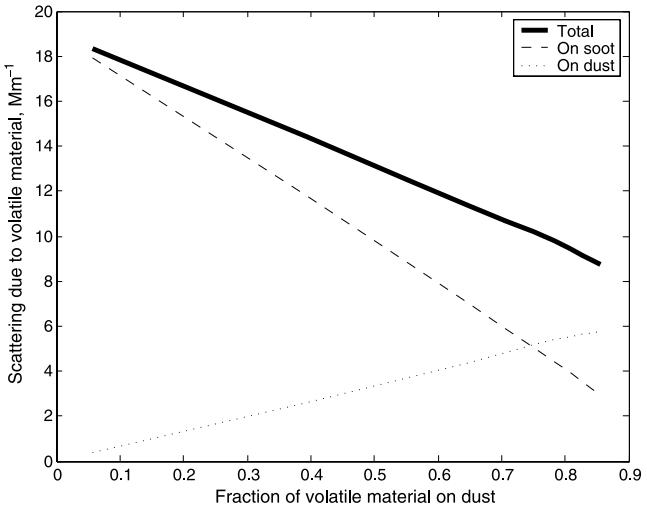

Figure 12. Modeled effect of dust on scattering by the volatile fraction, defined as the total scattering minus scattering due to soot and dust.

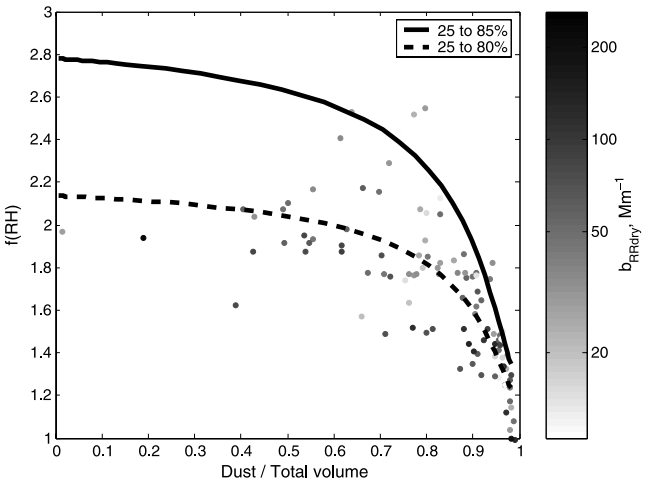

Figure 13. Modeled and measured relationship between dust and *f*(RH). The lines show modeled *f*(RH) for two humidity spans, while the dots show the measurements.

[56] **Acknowledgments.** We would like to thank the staff at the NCAR Research Aviation Facility, who were unfailingly helpful through the entire project and are always a pleasure to work with. The particle sizing and counting work was supported by NSF (grant ATM00-02070). The MOI and OC/EC work was supported by NSF grant ATM00-02698 and amendments thereto. T. L. Anderson and S. J. Doherty acknowledge support from the National Science Foundation (grants ATM-0002198 and ATM-0138250). This research is a contribution to the International Global Atmospheric Chemistry core project of the International Geosphere-Biosphere Program. This is SOEST contribution 6633.

References

Adams, P. J., and J. H. Seinfeld (2002), Predicting global aerosol size distributions in general circulation models, *J. Geophys. Res.*, *107*(D19), 4370, doi:10.1029/2001JD001010.

Anderson, T. L., and J. A. Ogren (1998), Determining aerosol radiative properties using the TSI 3563 intergrating nephelometer, *Aerosol Sci. Technol.*, *29*, 57–69.

Anderson, T. L., S. J. Masonis, D. S. Covert, N. C. Ahlquist, S. G. Howell, A. D. Clarke, and C. S. McNaughton (2003), Variability of aerosol optical properties derived from in situ aircraft measurements during ACE-Asia, *J. Geophys. Res.*, *108*(D23), 8647, doi:10.1029/2002JD003247.

Bohren, C. F., and D. R. Huffman (1983), *Absorption and Scattering of Light by Small Particles*, Wiley-Interscience, Hoboken, N. J.

Bond, T. C., T. L. Anderson, and D. Campbell (1999), Calibration and intercomparison of filter-based measurements of visible light absorption by aerosols, *Aerosol Sci. Technol.*, *30*, 582–600.

Carrico, C. M., P. Kus, M. J. Rood, P. K. Quinn, and T. S. Bates (2003), Mixtures of pollution, dust, sea salt, and volcanic aerosol during ACE-Asia: Radiative properties as a function of relative humidity, *J. Geophys. Res.*, *108*(D23), 8650, doi:10.1029/2003JD003405.

Chen, Z., A. Taflove, and V. Backman (2003), Equivalent volume-averaged light scattering behavior of randomly inhomogeneous dielectric spheres in the resonant range, *Opt. Lett.*, *28*(10), 756–767.

Clarke, A. D. (1989), In-situ measurements of the aerosol size distributions, physicochemistry and light absorption properties of Arctic haze, *J. Atmos. Chem.*, *9*(1–3), 255–266.

Clarke, A. D. (1991), A thermo-optic technique for in situ analysis of size-resolved aerosol physicochemistry, *Atmos. Environ., Part A*, *25*, 635–644.

Clarke, A. D., et al. (2002), INDOEX aerosol: A comparison and summary of chemical, microphysical, and optical properties from land, ship, and aircraft, *J. Geophys. Res.*, *107*(D19), 8033, doi:10.1029/2001JD000572.

Clarke, A. D., et al. (2004), Size distributions and mixtures of dust and black carbon aerosol in Asian outflow: Physiochemistry and optical properties, *J. Geophys. Res.*, *109*, D15S09, doi:10.1029/2003JD004378.

Cohen, M. D., R. C. Flagan, and J. H. Seinfeld (1987), Studies of concentrated electrolyte solutions using the electrodynamic balance: 2. Water activities for mixed-electrolyte solutions, *J. Phys. Chem.*, *91*, 4575–4582.

Ding, Y., Y. Pang, and D. J. Eatough (2002), High-volume diffusion denuder sampler for the routine monitoring of fine particulate matter: 1. Design and optimization of the PC-BOSS, *Aerosol Sci. Technol.*, *36*, 369–382.

Doherty, S. J., P. K. Quinn, A. Jefferson, C. M. Carrico, T. L. Anderson, and D. Hegg (2005), A comparison and summary of aerosol optical properties as observed in situ from aircraft, ship, and land during ACE-Asia, *J. Geophys. Res.*, *110*, D04201, doi:10.1029/2004JD004964.

Fuller, K. A., W. C. Malm, and S. M. Kreidenweis (1999), Effects of mixing on extinction by carbonaceous particles, *J. Geophys. Res.*, *104*(D13), 15,941–15,954.

Gao, Y., and J. R. Anderson (2001), Characteristics of Chinese aerosols determined by individual-particle analysis, *J. Geophys. Res.*, *106*(D16), 18,037–18,046.

Gasparini, R., R. Li, and D. R. Collins (2004), Integration of size distributions and size-resolved hygroscopicity measured during the Houston Supersite for compositional categorization of the aerosol, *Atmos. Environ.*, *38*, 3285–3303.

Howell, S. G., and B. J. Huebert (1998), Determining marine aerosol scattering characteristics at ambient humidity from size-resolved chemical composition, *J. Geophys. Res.*, *103*(D1), 1391–1404.

Huebert, B. J., T. Bates, P. B. Russell, G. Y. Shi, Y. J. Kim, K. Kawamura, G. Carmichael, and T. Nakajima (2003), An overview of ACE-Asia: Strategies for quantifying the relationships between Asian aerosols and their climatic impacts, *J. Geophys. Res.*, *108*(D23), 8633, doi:10.1029/2003JD003550.

Huebert, B., T. Bertram, S. Howell, D. Eatough, J. Kline, and B. Blomquist (2004a), Measurements of organic and elemental carbon in Asian outflow during ACE-Asia from the NSF/NCAR C-130, *J. Geophys. Res.*, *109*, D19S11, doi:10.1029/2004JD004700.

Huebert, B. J., et al. (2004b), PELTI: Measuring the passing efficiency of an airborne low turbulence aerosol inlet, *Aerosol Sci. Technol.*, *38*, 803–826.

Im, J.-S., V. K. Saxena, and B. N. Wenny (2001), An assessment of hygroscopic growth factors for aerosols in the surface boundary layer for computing direct radiative forcing, *J. Geophys. Res.*, *106*(D17), 20,213–20,224.

Intergovernmental Panel on Climate Change (2001), Third assessment report of the Intergovernmental Panel on Climate Change, technical report, Geneva, Switzerland, Jan.

Kalashnikova, O. V., and I. N. Sokolik (2002), Importance of shapes and compositions of wind-blown dust particles for remote sensing at solar wavelengths, *Geophys. Res. Lett.*, *29*(10), 1398, doi:10.1029/2002GL014947.

Kapustin, V. N., A. D. Clarke, Y. Shinozuka, S. Howell, V. Brekhovskikh, T. Nakajima, and A. Higurashi (2006), On the determination of a cloud condensation nuclei from satellite: Challenges and possibilities, *J. Geophys. Res.*, *111*, D04202, doi:10.1029/2004JD005527.

Kline, J., B. Huebert, S. Howell, B. Blomquist, J. Zhuang, T. Bertram, and J. Carillo (2004), Aerosol composition and size versus altitude measured from the C-130 during ACE-Asia, *J. Geophys. Res.*, *109*, D19S08, doi:10.1029/2004JD004540.

Kotchenruther, R. A., P. V. Hobbs, and D. A. Hegg (1999), Humidification factors for atmospheric aerosols off the mid-Atlantic coast of the United States, *J. Geophys. Res.*, *104*(D2), 2239–2251.

Kus, P., C. M. Carrico, M. J. Rood, and A. Williams (2004), Measured and modeled light scattering values for dry and hydrated laboratory aerosols, *J. Atmos. Oceanic Tech.*, *21*, 981–994.

Lee, Y.-N., et al. (2003), Airborne measurement of inorganic ionic components of fine aerosol particles using the PILS-IC technique during ACE-Asia and TRACE-P, *J. Geophys. Res.*, *108*(D23), 8646, doi:10.1029/2002JD003265.

Li-Jones, X., H. B. Maring, and J. M. Prospero (1998), Effect of relative humidity on light scattering by mineral dust aerosol as measured in the marine boundary layer over the tropical Atlantic Ocean, *J. Geophys. Res.*, *103*(D23), 31,113–31,122.

Maria, S. F., L. M. Russell, B. J. Turpin, R. J. Porcja, T. L. Campos, R. J. Weber, and B. J. Huebert (2003), Source signatures of carbon monoxide and organic functional groups in Asian Pacific regional aerosol characterization experiment (ACE-Asia) submicron aerosol types, *J. Geophys. Res.*, *108*(D23), 8637, doi:10.1029/2003JD003703.

Markowicz, K. M., P. J. Flatau, P. K. Quinn, C. M. Carrico, M. K. Flatau, A. M. Vogelmann, D. Bates, M. Liu, and M. J. Rood (2003), Influence of relative humidity on aerosol radiative forcing: An ACE-Asia experiment perspective, *J. Geophys. Res.*, *108*(D23), 8662, doi:10.1029/2002JD003066.

Massling, A., A. Wiedensohler, B. Busch, C. Neususs, P. Quinn, T. Bates, and D. Covert (2003), Hygroscopic properties of different aerosol types over the Atlantic and Indian oceans, *Atmos. Chem. Phys.*, *3*, 1377–1397.

Mayol-Bracero, O. L., R. Gabriel, M. O. Andreae, T. W. Kirchstetter, T. Novakov, J. Ogren, P. Sheridan, and D. G. Streets (2002), Carbonaceous aerosols over the Indian Ocean during the Indian Ocean Experiment (INDOEX): Chemical characterization, optical properties, and probable sources, *J. Geophys. Res.*, *107*(D19), 8030, doi:10.1029/2000JD000039.

McNaughton, C. S., et al. (2004), Spatial distribution and size evolution of particles in Asian outflow: Significance of primary and secondary aerosols during ACE-Asia and TRACE-P, *J. Geophys. Res.*, *109*, D19S06, doi:10.1029/2003JD003528.

Ming, Y., and L. M. Russell (2002), Thermodynamic equilibrium of organic-electrolyte mixtures in aerosol particles, *AIChE J.*, *48*, 1331–1348.

Pitchford, M. L., and P. H. McMurry (1994), Relationship between measured water vapor growth and chemistry of atmospheric aerosol for Grand Canyon, Arizona, in winter 1990, *Atmos. Environ.*, *28*, 827–840.

Rader, D. J., and P. H. McMurry (1986), Application of the tandem differential mobility analyzer to studies of droplet growth or evaporation, *J. Aerosol Sci.*, *17*(5), 771–787.

Reid, E. A., J. S. Reid, M. M. Meier, M. R. Dunlap, S. S. Cliff, A. Broumas, K. Perry, and H. Maring (2003), Characterization of African dust transported to Puerto Rico by individual particle and size segregated bulk analysis, *J. Geophys. Res.*, *108*(D19), 8591, doi:10.1029/2002JD002935.

Reid, J. S., et al. (2003), Comparison of size and morphological measurements of coarse mode dust particles from Africa, *J. Geophys. Res.*, *108*(D19), 8593, doi:10.1029/2002JD002485.

Seinfeld, J. H., and S. N. Pandis (1998), *Atmospheric Chemistry and Physics: From Air Pollution to Climate Change*, Wiley-Interscience, Hoboken, N. J.

Swietlicki, E., et al. (2000), Hygroscopic properties of aerosol particles in the north eastern Atlantic during ACE 2, *Tellus, Ser. B*, *52*, 201–227.

Tang, I. N., A. C. Tridico, and K. H. Fung (1997), Thermodynamic and optical properties of sea salt aerosols, *J. Geophys. Res.*, *102*(D19), 23,269–23,275.

Tang, Y., et al. (2004), The impacts of dust on regional tropospheric chemistry during the ACE-Asia experiment: A model study, *J. Geophys. Res.*, *109*, D19S21, doi:10.1029/2003JD003806.

Twomey, S. (1977), *Atmospheric Aerosols*, Elsevier, New York.

Weast, R. C., D. R. Lide, M. J. Astle, and W. H. Beyer (Eds.) (1989), *CRC Handbook of Chemistry and Physics*, 70th ed., CRC Press, Boca Raton, Fla.

Winchester, J. W., and W. Ming-Xing (1989), Acid-base balance in aerosol components of the Asia-Pacific region, *Tellus, Ser. B*, *41*, 323–337.

Winklmayr, W., H.-C. Wang, and W. John (1990), Adaptation of the Twomey algorithm to the inversion of cascade impactor data, *Aerosol Sci. Technol.*, *13*, 322–331.

T. L. Anderson and S. J. Doherty, Department of Atmospheric Sciences, University of Washington, Box 351640, Seattle, WA 98195-1640, USA.

A. D. Clarke, S. G. Howell, B. J. Huebert, V. Kapustin, C. S. McNaughton, and Y. Shinozuka, School of Ocean and Earth Science and Technology, University of Hawaii at Manoa, Honolulu, HI 96822, USA. (showell@soest.hawaii.edu)